# Sustainable Hybrid Energy Harvester based on Air Stable Quantum Dot Solar Cells and Triboelectric Generator

*Yuljae Cho,[a,†] Sanghyo Lee,[a,†] John Hong,[a] Sangyeon Pak,[a] Bo Hou,[a] Young-Woo Lee,[b] Jae Eun Jang,[c] Hyunsik Im,[d] Jung Inn Sohn,[d,*] SeungNam Cha,[a,*] Jong Min Kim[e]*

[a]*Department of Engineering Science, University of Oxford, Parks Road, Oxford OX1 3PJ, United Kingdom*

[b]*Department of Energy Systems, Soonchunhyang University, Asan, Chungcheongnamdo, 31538, Republic of Korea*

[c]*Department of Information and Communication Engineering, Daegu Gyeongbuk Institute of Science and Technology, Daegu, Republic of Korea*

[d]*Division of Physics and Semiconductor Science, Dongguk University, Seoul 100-715, Republic of Korea*

[e]*Department of Engineering, University of Cambridge, 9 JJ Thomson Avenue, Cambridge CB3 0FA, United Kingdom*

[†]These authors contributed equally to this work

*Corresponding authors: junginn.sohn@dongguk.edu, seungnam.cha@eng.ox.ac.uk

**Abstract**

Realization of self-powered sensor systems is the key technology to accomplish internet of things technology for smart life of a human being. Recent advances in energy harvesting using photovoltaic and triboelectric effects demonstrate outstanding performances of energy harvesters as power supply. However, there are still fundamental issues to be dealt with in details which are neglected so far, such as power interruption due to intermittence of natural energy and a long-term device stability in air. In this report, we demonstrate a hybrid energy harvester (HEH) that is composed of high air stable quantum dots solar cells (QDSCs) and triboelectric energy generator (TENG). The HEH demonstrates dual mode as well as simultaneous energy harvesting with respect to types of energy present. Attributed to high photocurrent and high potential from QDSCs and the TENG, immediate base power followed by steady enhancement in power generation is achieved in a hybrid system. The HEH demonstrates as a stable power supply to accomplish a sustainable sensor system without the aid of any external power supply.

**Introduction**

In the new era of smart life, internet of things (IoT), which autonomously performs sensing, networking and communicating between objects, is an indispensable technology to improve quality of life for a human being.[1-3] In this regard, it is of prime importance to construct a reliable and a sustainable sensor system, such as an integrated sensor for healthcare, environment monitoring, and building management, in order to realize the IoT technology.[4-6] In particular, sustainability of a sensor system is one of the prerequisite requirements to extend a service area of a sensor network and to ensure reliability of the sensor network system.[7-9] Recent advances in energy harvesting technology, which utilizes the photovoltaic and triboelectric effect to convert environmentally abundant energy to electrical one, shows a promise of realization of a sustainable sensor network. For example, an energy harvesting technology demonstrated a self-powered sensor system with the aid of a storage device.[10-17]

In spite of steady progress in the area of energy harvesting,[18-21] there are still fundamental issues to be discussed in details which have been neglected. Due to intermittence of environmental energy sources, sole dependence on one type of an energy source may cause a sudden interruption to power supply. In addition, an energy harvester suffers from low potential or current due to its unique physical effect, such as photovoltaic and triboelectric effect, respectively, which is a critical shortcoming of the energy harvester for practical applications. Lastly, long-term device stability in an air ambient condition is an essential standard for the energy harvester to provide stable power.

Here, we introduce a hybrid energy harvester (HEH), which performs dual mode as well as simultaneous energy harvesting with long-term stability up to 140 days in ambient air. In particular, lead sulfide quantum dots (PbS QDs) are employed as a light absorbing material for photon energy harvesting because of their high air stability and high light absorption coefficient which ensures to generate high photocurrent.[11,12]. Furthermore, poly(vinylidenefluoride-trifluoroethylene-chlorotrifluoroethylene) (P(VDF-TrFE-CTFE), is used for a triboelectric generator (TENG) because CTFE has shown high transparency, ensuring light penetration to QDSCs, high potential generation, and high mechanical stability.[14]

In a hybrid system, high photocurrent from QD solar cells (QDSCs) enables to generate immediate base power. Generation of power is then steadily enhanced beyond the power limited by an

open circuit voltage ($V_{oc}$) of the QDSCs, which is attributed to high potential from the TENG. In addition, the HEH demonstrated applications to self-powered systems, such as a generation of an optical signal using light emitting diodes (LEDs) and an operation of an infrared (IR) sensor without the aid of external power supply, which shows a promise of realization of IoT technology using hybrid energy harvesting.

**Results and discussion**

Figure 1(a) illustrates a structure of a HEH which is composed of 6 cells of PbS QDSCs connected in series and a TENG. In order to fabricate the HEH, we used a solution-based process to prevent possible damages to the harvesters caused by a high temperature treatment. For photon energy harvesting, PbS QDs in a solution phase were synthesized as described in our previous work.[12] To determine a bandgap of PbS QDs, we employed ultraviolet and visible absorption spectroscopy (UV-Vis). As shown in Figure 1(b) (left), the first exciton peak was observed at 1000 nm corresponding to a bandgap of 1.24 eV. In addition, crystallographic characterization using high resolution transmission electron microscopy (HRTEM) was performed. Figure 1(b) (right) shows a typical rock-salt cubic crystalline structure of PbS QDs with an observation of a lattice fringe of (220). To fabricate PbS QDSCs, PbS QDs were sequentially treated by n-type tetrabutylammonium iodide (TBAI) and p-type 1,2-ethanedithiol (EDT) ligands (Figure 1(c)), which demonstrated remarkably long-time air stability in our previous reports.[22-24]

Then, a P(VDF-TrFE-CTFE) layer (which we will call CTFE afterwards) on a graphene electrode was transferred to the other side of the substrate. CTFE was employed because the CTFE exhibits high mechanical stability and excellent energy harvesting performance at wide-range of frequencies.[14,25,26] The top image of the Figure 1(d) describes a β-phase crystalline structure of CTFE where red arrows indicate a direction of dipole polarization.[27-29] The β-phase CTFE is formed by a solvent annealing (SA) method (Figure 1(d)-bottom).[14] Detailed fabrication processes are described in the Experimental section.

Because the TENG and QDSCs are assembled in a vertical manner to maximize an active area of each device in order to generate higher current and potential, light transmittance of the TENG is one

of the important criteria. Figure 1(e) shows that a transmittance of the TENG (a β-phase CTFE layer on a graphene electrode) is approximately 95%,[30,31] which suggests that most of photon energy will reach to PbS QD layers. The high transparency of the CTFE layer is attributed to the surface flattening effect of SA, which reduces light scattering at the surface of the polymer film as evidenced by color tuning of the film as shown in Figure 1(f) (top).[13] The digital images of a fabricated HEH is shown in Figure 1(f) (bottom). PbS QDs were uniformly coated over the entire substrate with the size of 2.5 by 2.5 $cm^2$ and a TENG exhibited high transparency.

To comprehensively investigate the HEH and its potential use for sustainable sensor networks, first, a performance of an individual component (QDSCs and then the TENG) was studied. Attributed to a high light absorption coefficient of PbS QDs, single QDSC exhibited high short circuit current ($I_{sc}$) of approximately $(7.82 \pm 0.096) \times 10^{-4}$ A, corresponding to short circuit current density ($J_{sc}$) of 26.06 ± 0.32 $mA/cm^2$ as shown in Figure 2(a) and Supplementary Table S1. However, open circuit voltage ($V_{oc}$) of the QDSC turned out to be 0.51 ± 0.01 V and this relatively low $V_{oc}$ overshadowed benefits of high photocurrent. In order to increase a potential limit, PbS QDSCs on a patterned ITO were connected in series. As shown in Figure 2(a) and (b), QDSCs in a series connection showed gradually enhanced $V_{oc}$ whereas a decrease in $I_{sc}$ was observed due to increased series resistance ($R_s$). In spite of a trade-off between $I_{sc}$ and $V_{oc}$, it is apparent that $V_{oc}$ improvement was noticeable compared to $I_{sc}$, which, in turn, led to increase amount of power generated by the QDSCs.

A performance of the 6 QDSCs that were connected in series (6-QDSCs afterwards) before and after assembly of the TENG was characterized as shown in Figure 2(c). Slight decrease in $I_{sc}$ from $7.18 \times 10^{-4}$ A ($J_{sc}$ ~ 23.9 $mA/cm^2$) to $6.65 \times 10^{-4}$ A ($J_{sc}$ ~ 22.1 $mA/cm^2$) was observed in the HEH, i.e. after assembly of the TENG, which is due to slight decrease in light transmittance (Figure 1(e)). Nevertheless, changes of PCE were negligible, ~ 0.1% (Supplementary Table S2). In addition, PbS QDSCs exhibited high air stability up to 140 days (20 weeks) without any encapsulation as shown in Figure 2(d). Above results suggest that our device configuration is a desirable approach to achieve a hybrid energy harvesting system for sustainable sensor networks.

Performances of the TENG were evaluated by using mechanical energy sources, such as vibrations, sound, and wind. Figure 3(a) illustrates schematics of the TENG working mechanism. In a steady state, negative charges are induced on the surface of a CTFE film due to dipole polarization.[14] When mechanical energy is applied to a top electrode, positive charges are induced at the top electrode because of relative potential difference between the top electrode and the polymer surface, which leads to induce negative charges at the bottom electrode (Figure 3a-(i)). Therefore, electrons are transported to the top electrode until the top electrode contacts the terpolymer film (Figure 3a-(ii)). Conversely, electrons moved to the top electrode transport back to the bottom electrode to offset potential difference between the top and the bottom electrodes when the top electrode is released (Figure 3a-(iii) and (iv)).[32-37] Figure 3(b) and (c) show potential and current output of the TENG after rectification, respectively. The TENG was driven by mechanical vibrations at the frequency of 50 Hz and an input force of 0.5 N per vibration. In addition, potential and current output without rectification at the frequency ranging from 10 to 50 Hz are shown in Supplementary Figure S1.

The stability of the TENG was tracked by periodically measuring output performances, which exhibited stable performances up to 140 days in ambient air as shown in Figure 3(d). Long-term stability of the PbS QDSCs (Figure 2(d)) and the TENG (Figure 3(d)) promises realization of a high air stable hybrid energy harvesting device for a sustainable sensor system. In addition, the TENG demonstrated that various types of mechanical energy sources, such as sound and wind, could be readily harvested. As shown in Figure 3(e) (left), the TENG was held using optics apparatus, and then sound and wind waves were applied. Intensity of sound was set to within the range of 80 ~ 90 dB which is similar to intensity of sound from a vacuum cleaner. To generate wind waves, we employed an office fan with a diameter of approximately 35 cm. Figure 3(e) summarizes output performances of harvesting sound and wind waves and also potential and current output curves are shown in Supplementary Figure S2.

As shown in Figure 2 and 3, an individual component of the HEH demonstrated high performances and high air stability up to 140 days. In addition, given two distinct features of energy harvesters, i.e. high potential of the TENG and high current of the 6-QDSCs, one can be an ideal complement to the other and *vice versa* when those energy harvesters are hybridized together. High

current from the QDSCs immediately generates base power which is gradually added up over potential limit of the QDSCs ($V_{oc}$) by higher potential of the TENG. In addition, hybridization of energy harvesters provides more stable and reliable device performance as it is able to harvest different types of environmental energy sources simultaneously, which reduces risks of power interruption due to intermittence of the environmental energy.

In order to efficiently manage output signals from the HEH, a power management circuit (Supplementary Figure S3(a)) was employed. Supplementary Figure S3(b) illustrates an electricity flow diagram of the TENG when two energy harvesters are connected in series. It is worth noting that the HEH with a series connection is beneficial to enhance an output voltage of the device, which is one of the important parameters for energy harvesters to meet an operation voltage of an energy consuming device.

As shown in Figure 4(a), the HEH demonstrated dual mode as well as simultaneous energy harvesting with respect to types of energy sources; harvesting only photons (region ‘i' in blue), both photons and mechanical vibrations simultaneously (region ‘ii’ in purple), and only mechanical vibrations (region ‘iii’ in red), respectively. Followed by studies on characteristic output performances of the integrated system, an ability of the HEH to deliver power with respect to types of energy sources was investigated using the power management circuit equipped with capacitors (200 μF). As the same as the measurement in Figure 4(a), three different kinds of characterizations were performed using only photons, mechanical vibrations or simultaneous input of photons and mechanical vibrations. As depicted in yellow in Figure 4(b), the 6-QDSCs immediately charged the capacitors to approximately 3 V when the light was on, which is attributed to their high current level of the QDSCs. However, maximum potential in the capacitors was limited to ~ 3 V ($V_{oc}$ of the 6-QDSCs) no matter how long the capacitors were charged. In contrast, potential in the capacitors (green) constantly increased during a period of a measurement when the TENG was driven by the mechanical vibrations, which indicates an upper potential limit of the whole system can be enhanced by the higher potential output of the TENG.

As we expected, the HEH exhibited complimentary and synergetic effects when both photons and mechanical vibrations were simultaneously harvested. An initial rapid rise of potential in the capacitors by the 6-QDSCs was followed by a constant increase (red) over potential that could not be attained by any individual component within the same period of time. Potential values were found to be 2.6, 7.5 and 11 V and also the charging speed per second were 14, 40, and 58 mV/sec for the 6-QDSCs, TENG and HEH, respectively.

As proof of concept, we demonstrated the potential applications of the HEH; first, generating optical signals using commercialized LEDs, and second operating an IR sensor. As shown in Supplementary Video S1 and S2, 6 blue LEDs connected in series were successfully lit up by the HEH at various conditions such as different charging and switching periods. Considering that a turn-on voltage of 6 blue LEDs is over 10 V (1.8 V each), the result demonstrates generation of large amount of potential and an enhanced charging speed.

In addition, the application to a sustainable sensor system was demonstrated using a commercialized IR sensor. The IR sensor was connected with the power management circuit without any external power supply as shown in Supplementary Figure S3(c). The HEH converted incident light and mechanical vibrations into electric energy which was stored in capacitors (35 mF). The total amount of energy stored in the capacitors was approximately 215 mJ, corresponding to power of 59.7 μW, which is in a good agreement with the power (60.5 μW) that was calculated by the potential curve in Figure 4(b). As shown in Figure 4(c) and Supplementary Video S3, the embedded chip LED in the IR sensor was alarmed when IR was detected (Figure 4(d)). It is worth to note that because the commercialized IR sensor consumed mW scale power to drive, an employment of low power sensors in a micro- to nanowatt scale would further improve duration and reliability of a sensor network system. Above results highlight that the HEH is able to perform as a stable power source for building a sustainable sensor network to realize smart life of a human being.

**Conclusion**

In summary, the HEH, which consisted of the high air stable QDSCs and TENG, was fabricated by a solution-based process at room temperature in an ambient air condition. Individual components

demonstrated excellent energy conversion performances by harvesting various environmental energy sources, such as sunlight, mechanical vibrations, sound waves, and wind. In a hybrid system, the HEH demonstrated dual mode energy harvesting with respect to types of energy applied to, such as photons and mechanical vibrations. In addition, we observed complementary and synergetic effects of the HEH when various energy sources were simultaneously harvested. High current from the QDSCs rapidly produced base power and high potential of the TENG enabled the HEH to generate higher potential than any individual component. Attributed to the synergetic effect of the QDSCs and TENG, the hybrid system demonstrated faster capacitor charging speed and attained higher potential in the capacitors than those of individual components. Lastly, the HEH, as a sustainable and stable power supply, demonstrated generation of optical signals and operation of the IR sensor for realizing IoT technology for smart life of a human being.

**Experimental Section**

*Nanocrystal Synthesis:* Zinc oxide (ZnO) nanoparticles and lead sulfide (PbS) quantum dots were synthesized as described in elsewhere.[12]

*QDSC Fabrication:* A solution of ZnO nanoparticles in chloroform was spin-coated onto patterned ITO glass substrates at 3000 rpm for 30 seconds. Subsequently, one drop of PbS QDs solution was spin-coated at 3000 rpm. For the solid-state ligand exchange of PbS QDs layers, TBAI solution in methanol with concentration of 10 $mgml^{-1}$ was loaded and held for 30 seconds, which was followed by two times washing processes with methanol. EDT (0.02 vol% in acetonitrile) was treated by using direct coating method without loading time, followed by 2 times of acetonitrile washing. Fabricated QDSC was consisted of 8 layers of TBAI and 2 layers of EDT, which was deposited by a layer-by-layer spin-coating method. Thickness of QD layers was approximately 300 nm. Gold electrode with 100 nm thickness was deposited by thermal evaporation in high vacuum.

*TENG Fabrication:* P(VDF-TrFE-CTFE) powder (PVDF:TrFE:CTFE = 62:31:7 in Mole %) was purchased from PIEZOTECH ARKEMA and dissolved in 2-Butanone (ACS reagent, ≥ 99 %, Sigma Aldrich) at a concentration of 10 wt%. The solution was stirred for one day at room temperature and then stirred for one to two hours before it was used. Then, P(VDF-TrFE-CTFE) solution was spin-coated at 500 rpm for 10 seconds and then 3000 rpm for 40 seconds on a graphene electrode on Cu foil which was synthesized by a chemical vapor deposition (CVD) method.[38] To treat a solvent annealing process, samples were placed on a sample holder in a closed chamber with 2-Butanone underneath the sample holder. Solvent annealing was applied to the film for 30 min per 1 μm right after spin-coating.[13,14] Then, the samples were dried to remove the solvent from inside of the film and Cu foil was etched by using 0.2 M of ammonium persulfate solution. Drying transfer method was used to assemble a TENG with QDSCs. The size of HEH was 2.5 by 2.5 $cm^2$.

## Author contributions

Y.C., S.L and S.C. conceived the experiments and led the project. J.H and B.H. performed the material synthesis and characterisation. S.P. and Y. L carried out the device fabrication and characterisation. S.D. J.J. and H.I. contributed to scientific discussion and provided experimental guidance. J.S. and J.K. contributed to the interpretation of the data and commented on the manuscript. Y.C and S.C. wrote the paper with input and discussion from all authors.

**Acknowledgement**

This work was supported by a grant from National Research Foundation of Korea (NRF) (2015M2A2A6A02045252, 2015R1A6A3A03017921). The research leading to these results received funding from European Commission Horizon2020 under grant agreement number (685758)

**References**

(1) R. Minerva, A. Biru, and D. Rotondi, *IEEE Internet Initiative,* 2015, **1**.

(2) X. He, Y. Zi, H. Yu, S. L. Zhang, J. Wang, W. Ding, H. Zou, W. Zhang, C. Lu, and Z. L. Wang, *Nano Energy*, 2017, **39**, 328-336.

(3) Z. L. Wang, J. Chen, and L. Lin, *Energy Environ. Sci.*, 2015, **8**, 2250-2282.

(4) A. Ahmed, Z. Saadatnia, I. Hassan, Y. Zi, Y. Xi, X. He, J. Zu, and Z. L. Wang, *Adv. Energy Mater.*, 2017, **7**, 1601705.

(5) S. Wang, X. Wang, Z. L. Wang, and Y. Yang, *ACS Nano*, 2016, **10**, 5696-5700.

(6) Y. Ma, Q. Zheng, Y. Liu, B. Shi, X. Xue, W. Ji, Z. Liu, Y. Jin, Y. Zou, and Z. An, *Nano Lett.*, 2016, **16**, 6042-6051.

(7) S. Niu, X. Wang, F. Yi, Y. S. Zhou, and Z. L. Wang, *Nat. Commun.*, 2015, **6**, 8975.

(8) H. Guo, M. Yeh, Y. Lai, Y. Zi, C. Wu, Z. Wen, C. Hu, and Z. L. Wang, *ACS Nano*, 2016, **10**, 10580-10588.

(9) B. Zhang, J. Chen, L. Jin, W. Deng, L. Zhang, H. Zhang, M. Zhu, W. Yang, and Z. L. Wang, *ACS Nano*, 2016, **10**, 6241-6247.

(10) S. Li, J. Wang, W. Peng, L. Lin, Y. Zi, S. Wang, G. Zhang, and Z. L. Wang, *Adv. Energy Mater.*, 2017, **7**, 1602832.

(11) J. Hong, B. Hou, J. Lim, S. Pak, B. Kim, Y. Cho, J. Lee, Y. Lee, P. Giraud, S. Lee, J. B. Park, S. M. Morris, H. J. Snaith, J. I. Sohn, S. Cha, and J. M. Kim, *J. Mater. Chem. A*, 2016, **4**, 18769-18775.

(12) B. Hou, Y. Cho, B. Kim, J. Hong, J. B. Park, S. J. Ahn, J. I. Sohn, S. Cha, and J. M. Kim, *ACS Energy Lett.*, 2016, **1**, 834-839.

(13) Y. Cho, J. B. Park, B. Kim, J. Lee, W. Hong, I. Park, J. E. Jang, J. I. Sohn, S. Cha, and J. M. Kim, *Nano Energy*, 2015, **16**, 524-532.

(14) Y. Cho, D. Ahn, J. B. Park, S. Pak, S. Lee, B. O. Jun, J. Hong, S. Y. Lee, J. E. Jang, J. Hong, S. M. Morris, J. I. Sohn, S. N. Cha, and J. M. Kim, *Adv. Electron. Mater.*, 2016, **2**, 1600225.

(15) S. Lee, W. Ko, Y. Oh, J. Lee, G. Baek, Y. Lee, J. Sohn, S. Cha, J. Kim, J. Park, and J. Hong, *Nano Energy*, 2015, **12**, 410-418.

(16) L. Jin, W. Deng, Y. Su, Z. Xu, H. Meng, B. Wang, H. Zhang, B. Zhang, L. Zhang, X. Xiao, M. Zhu, and W. Yang, *Nano Energy*, 2017, **38**, 185-192.

(17) Y. Cho, P. Giraud, B. Hou, Y. Lee, J. Hong, S. Lee, S. Pak, J. Lee, J. E. Jang, S. M. Morris, J. I. Sohn, S. Cha, and J. M. Kim, *Adv. Energy Mater.*, 2018, **8**, 1700809.

(18) H. Shao, Z. Wen, P. Cheng, N. Sun, Q. Shen, C. Zhou, M. Peng, Y. Yang, X. Xie, and X. Sun, *Nano Energy*, 2017, **39**, 608-615.

(19) X. Pu, W. Song, M. Liu, C. Sun, C. Du, C. Jiang, X. Huang, D. Zou, W. Hu, and Z. L. Wang, *Adv. Energy Mater.*, 2016, **6**, 1601048.

(20) L. Zhang, B. Zhang, J. Chen, L. Jin, W. Deng, J. Tang, H. Zhang, H. Pan, M. Zhu, W. Yang, and Z. L. Wang, *Adv. Mater.*, 2016, **28**, 1650-1656.

(21) X. Wang, S. Wang, Y. Yang, and Z. L. Wang, *ACS Nano*, 2015, **9**, 4553-4562.

(22) C. M. Chuang, P. R. Brown, V. Bulović, and M. G. Bawendi, *Nat. Mater.*, 2014, **13**, 796-801.

(23) M. Liu, O. Voznyy, R. Sabatini, F. P. Garcia de Arquer, R. Munir, A. H. Balawi, X. Lan, F. Fan, G. Walters, A. R. Kirmani, S. Hoogland, F. Laquai, A. Amassian and E. H. Sargent, *Nat. Mater.*, 2016, **16**, 258–263

(24) Y. Cho, B. Hou, J. Lim, S. Lee, S. Pak, J. Hong, P. Giraud, A. Jang, Y. Lee, J. Lee, J. E. Jang, H. J. Snaith, S. M. Morris, J. I. Sohn, S. Cha, and J. M. Kim, *ACS Energy Lett.*, 2018, **3**, 1036-1043.

(25) J. Kim, J. H. Lee, H. Ryu, J. Lee, U. Khan, H. Kim, S. S. Kwak, and S. Kim, *Adv. Funct. Mater.*, 2017, **27**, 1700702.

(26) K. Y. Lee, S. K. Kim, J. Lee, D. Seol, M. K. Gupta, Y. Kim, and S. Kim, *Adv. Funct. Mater.*, 2016, **26**, 3067-3073.

(27) O. L. Smith, Y. Kim, M. Kathaperumal, M. R. Gadinski, M. Pan, Q. Wang, and J. W. Perry, *Appl. Mater. Interfaces*, 2014, **6**, 9584-9589.

(28) H. Gong, B. Miao, X. Zhang, J. Lu, and Z. Zhang, *RSC Adv.*, 2016, **6**, 1589-1599.

(29) Z. Li, J. Wang, X. Wang, Q. Yang, and Z. Zhang, *RSC Adv.*, 2015, **5**, 80950-80955.

(30) Y. Lee, G. An, B. Kim, J. Hong, S. Pak, E. Lee, Y. Cho, J. Lee, P. Giraud, S. N. Cha, H. Ahn, J. I. Sohn, and J. M. Kim, *ACS Appl. Mater. Interfaces*, 2016, **8**, 17651-17658.

(31) R. R. Nair, P. Blake, A. N. Grigorenko, K. S. Novoselov, T. J. Booth, T. Stauber, N. M. Peres, and A. K. Geim, *Science*, 2008, **320**, 1308.

(32) Q. Hua, J. Sun, H. Liu, R. Bao, R. Yu, J. Zhai, C. Pan, and Z. L. Wang, *Nat. Commun.*, 2018, **9**, 244.

(33) M. Xu, P. Wang, Y. Wang, S. L. Zhang, A. C. Wang, C. Zhang, Z. Wang, X. Pan, and Z. L. Wang, *Adv. Energy Mater.*, 2018, **26**, 1702432.

(34) K. Dong, Y. Wang, J. Deng, Y. Dai, S. L. Zhang, H. Zou, B. Gu, B. Sun, and Z. L. Wang, *ACS Nano*, 2017, **11**, 9490-9499.

(35) S. S. Kwak, H. Kim, W. Seung, J. Kim, R. Hinchet, and S. Kim, *ACS Nano*, 2017, **11**, 10733-10741.

(36) H. Ryu, J. Lee, T. Kim, U. Khan, J. Lee, S. S. Kwak, H. Yoon, and S. Kim, *Adv. Energy Mater.*, 2017, **6**, 1700289.

(37) S. S. Kwak, H. Kim, W. Seung, J. Kim, R. Hinchet, and S. Kim, *ACS Nano*, 2017, **11**, 10733-10741.

(38) X. Li, W. Cai, J. An, S. Kim, J. Nah, D. Yang, R. Piner, A. Velamakanni, I. Jung, E. Tutuc, S. K. Banerjee, L. Colombo, and R. S. Ruoff, *Science*, 2009, **324**, 1312-1314.

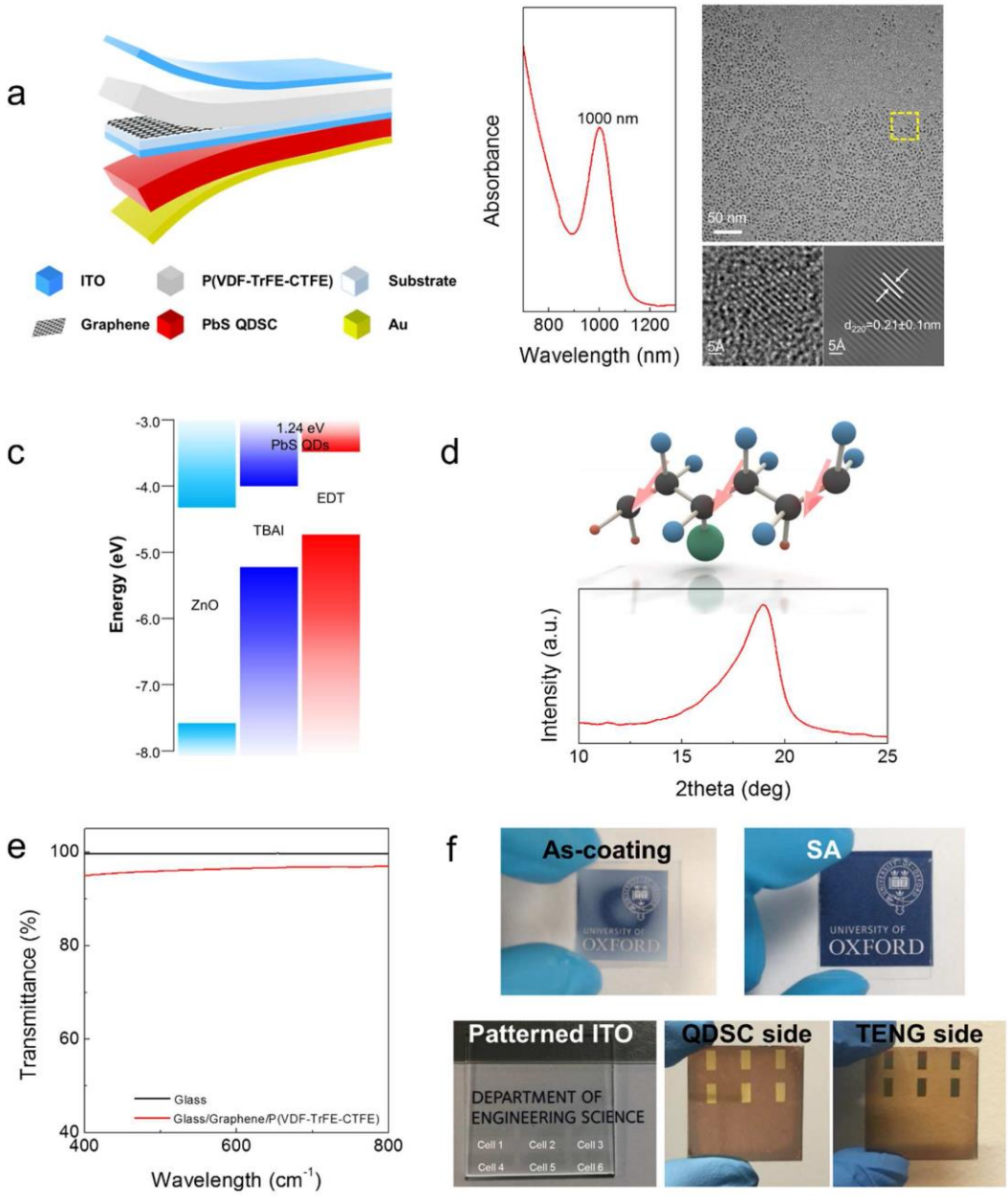


**Figure 1.** (a) Schematics of the hybrid energy harvester. (b) Absorption peak and HRTEM images of synthesized PbS QDs. (c) A structure of a QDSC. (d) A molecular structure of a β-phase P(VDF-TrFE-CTFE) film and XRD pattern of the film. (e) Comparison of transmittance of a glass substrate (black) with that of the TENG (red). (f) Pictures of before applying solvent annealing to the as-coated P(VDF-TrFE-CTFE) (top) and the fabricated hybrid energy harvester; a patterned ITO substrate (left), the QDSCs (middle), and the TENG (right).

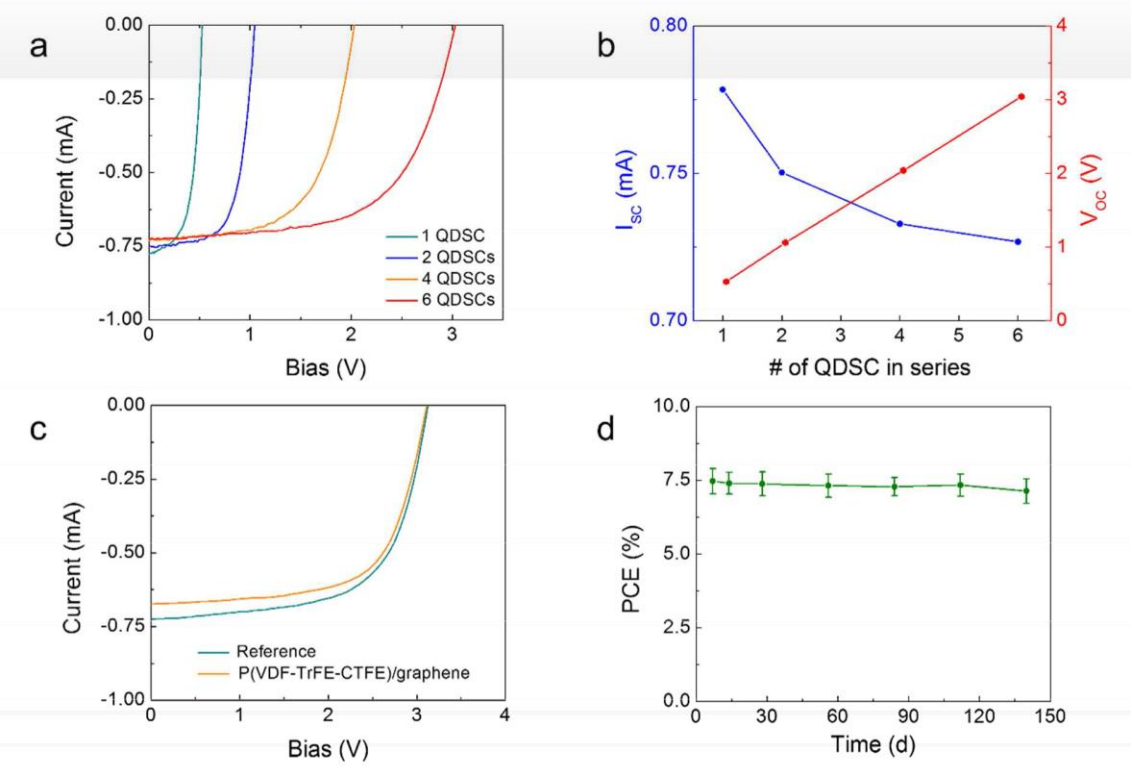


**Figure 2.** (a) I-V curves of QDSCs. (b) Short circuit current and open circuit voltage of QDSCs as a function of a number of QDSCs. (c) Comparison of 6-QDSCs performances before and after assembly of the TENG. (d) Air stability of QDSCs up to 140 days (20 weeks).

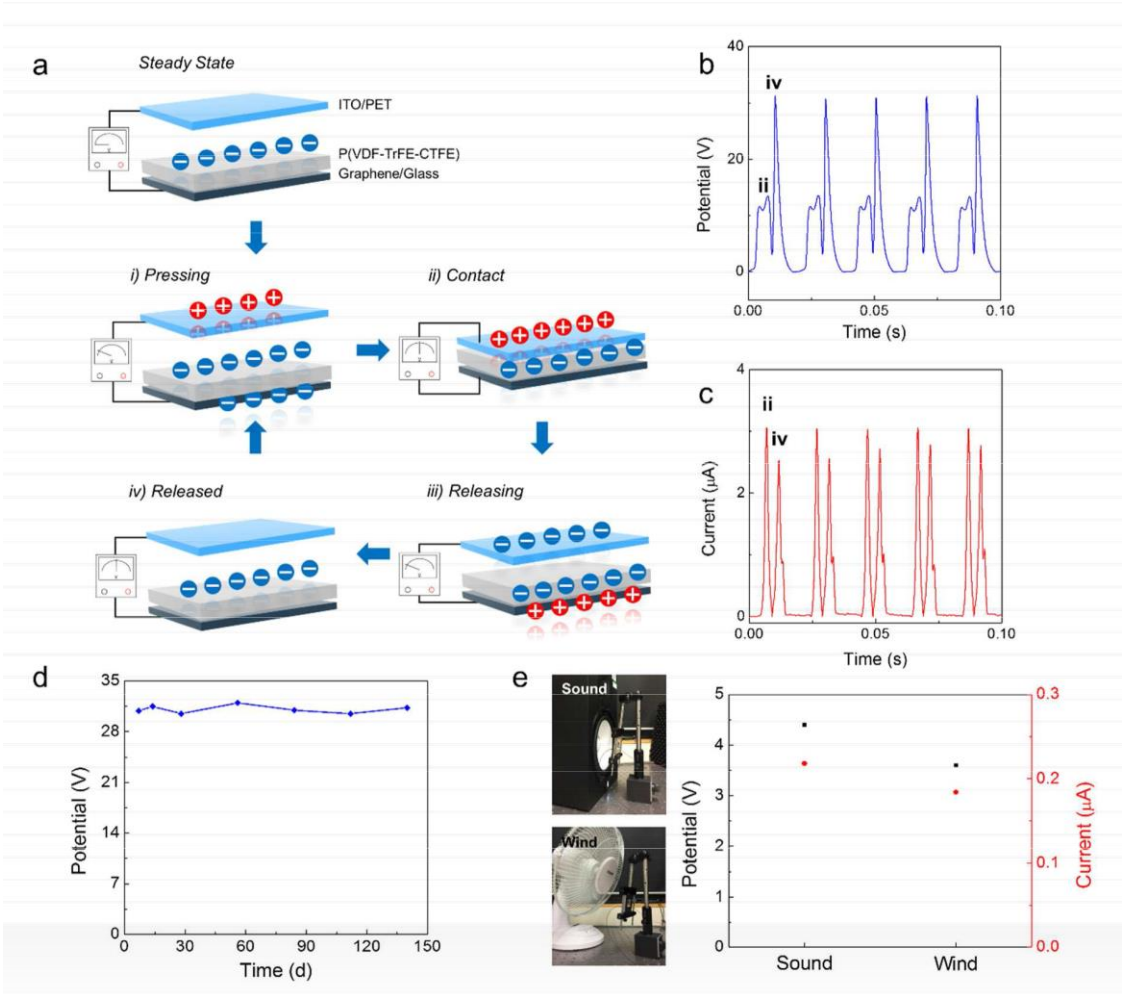


**Figure 3.** (a) Schematics of the TENG operation. (b) Potential and (c) current of the TENG at a frequency of 50 Hz. (d) Performances of the TENG over 140 days. (e) Digital images of experimental setting for sound and wind harvesting (left); potential and current output by harvesting sound and wind with a TENG, respectively (right).

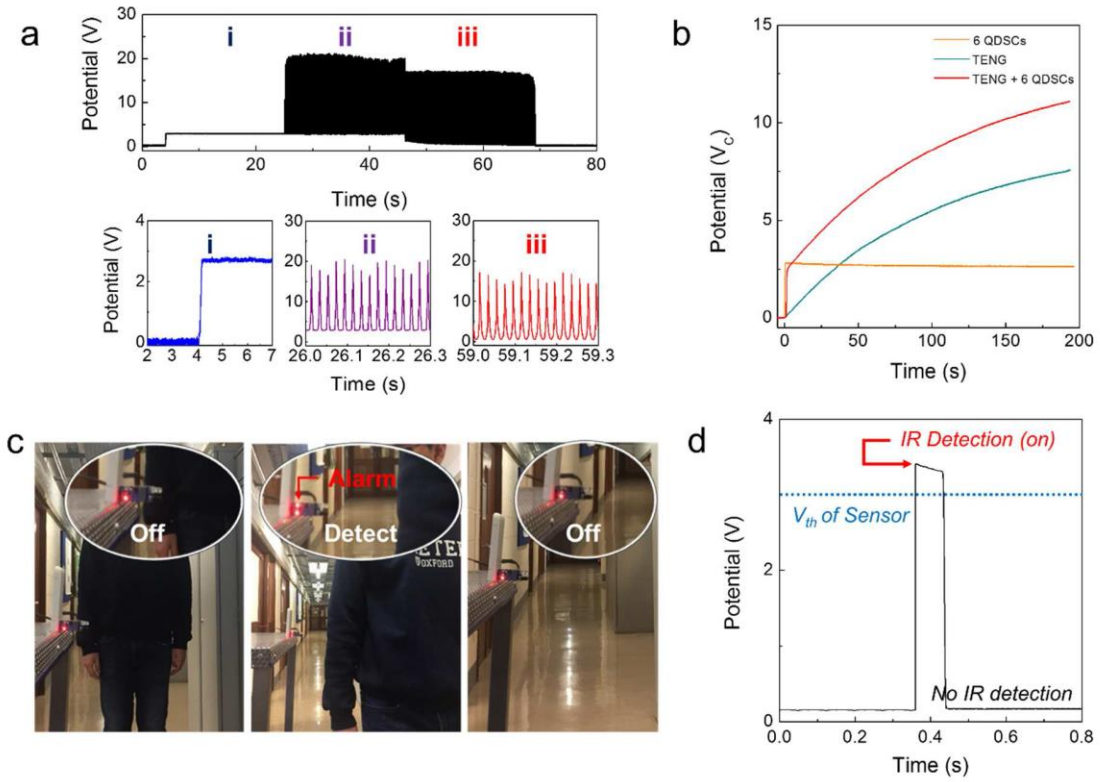


**Figure 4.** (a) Performances of the HEH by harvesting photons (i – blue), both energies simultaneously (photons and mechanical vibrations, ii – purple), and mechanical vibrations (iii – red), respectively. (b) Real-time potential measurement in capacitors by harvesting only photons (yellow), mechanical vibrations (light green), and both energies simultaneously (photons and mechanical vibrations, red). (c) A demonstration of an operation of an IR sensor that was powered by the HEH without any external power supply. (d) Potential read at the sensor when IR was detected.

**Supplementary Information**

# Sustainable Hybrid Energy Harvester based on Air Stable Quantum Dot Solar Cells and Triboelectric Generator

*Yuljae Cho,[a,†] Sanghyo Lee,[a,†] John Hong,[a] Sangyeon Pak,[a] Bo Hou,[a] Young-Woo Lee,[b] Jae Eun Jang,[c] Hyunsik Im,[d] Jung Inn Sohn,[d,*] SeungNam Cha,[a,*] Jong Min Kim[e]*

[a]*Department of Engineering Science, University of Oxford, Parks Road, Oxford OX1 3PJ, United Kingdom*

[b]*Department of Energy Systems, Soonchunhyang University, Asan, Chungcheongnamdo, 31538, Republic of Korea*

[c]*Department of Information and Communication Engineering, Daegu Gyeongbuk Institute of Science and Technology, Daegu, Republic of Korea*

[d]*Division of Physics and Semiconductor Science, Dongguk University, Seoul 100-715, Republic of Korea*

[e]*Department of Engineering, University of Cambridge, 9 JJ Thomson Avenue, Cambridge CB3 0FA, United Kingdom*

**Supplementary Table S1.** Individual performance of QDSCs.

| | | | | |
|---|---|---|---|---|
| 1 | 0.52 | 26.44 | 0.59 | 8.11 |
| 2 | 0.50 | 25.75 | 0.68 | 8.76 |
| 3 | 0.52 | 25.75 | 0.62 | 8.30 |
| 4 | 0.50 | 25.92 | 0.58 | 7.50 |
| 5 | 0.52 | 26.44 | 0.57 | 7.83 |
| 6 | 0.50 | 26.02 | 0.61 | 7.94 |
| Average | 0.51 ± 0.01 | 26.05 ± 0.32 | 0.61 ± 0.04 | 8.07 ± 0.43 |

**Supplementary Table S2.** Changes in power conversion efficiency of the 6-QDSCs before and after assembly of the TENG.

| Parameter | Before | After | Δ (After - Before) |
|---|---|---|---|
| $V_{oc}$ (V) | 3.12 | 3.12 | 0 |
| $J_{sc}$ (mA/cm$^2$) | 23.96 | 22.10 | -1.86 |
| FF | 0.61 | 0.65 | 0.04 |
| PCE | 7.60 | 7.47 | -0.13 |

Due to series connection, an active area of 6-QDSCs is 6 times larger than that of a single cell and thus PCE of the 6-QDSCs is calculated by using an equation below:

$$V_{oe} \times j_{se} \times FF / 6\,(\text{number of cells})$$

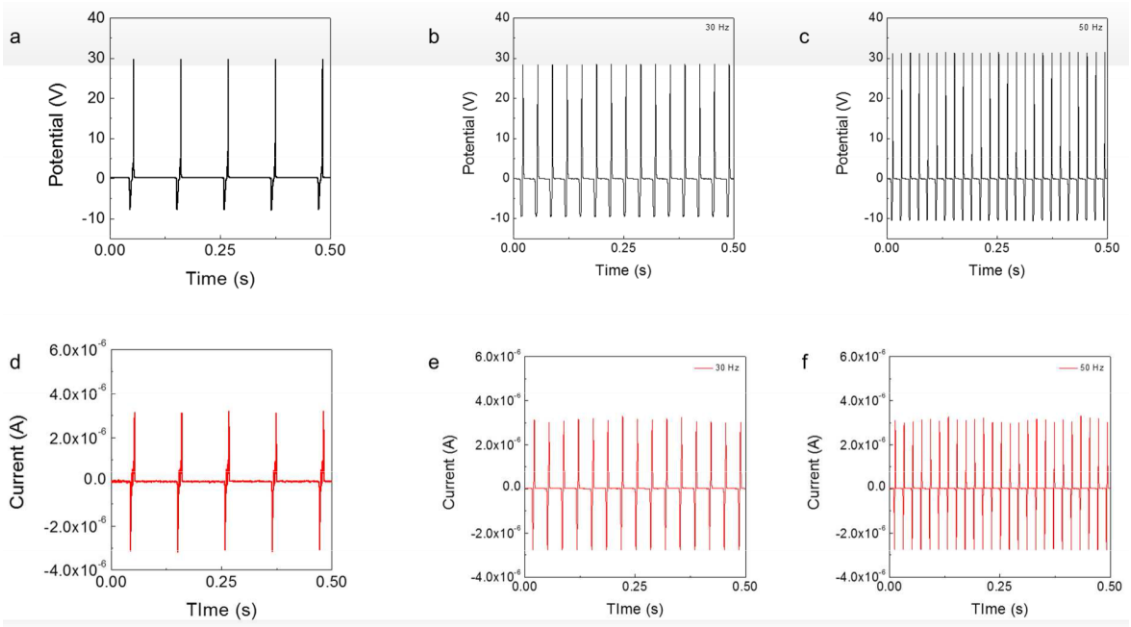


**Supplementary Figure S1**. Potential and current output of the TENG without rectification at the frequency of (a) and (d) 10 Hz, (b) and (e) 30 Hz, and (c) and (f) 50 Hz, respectively.

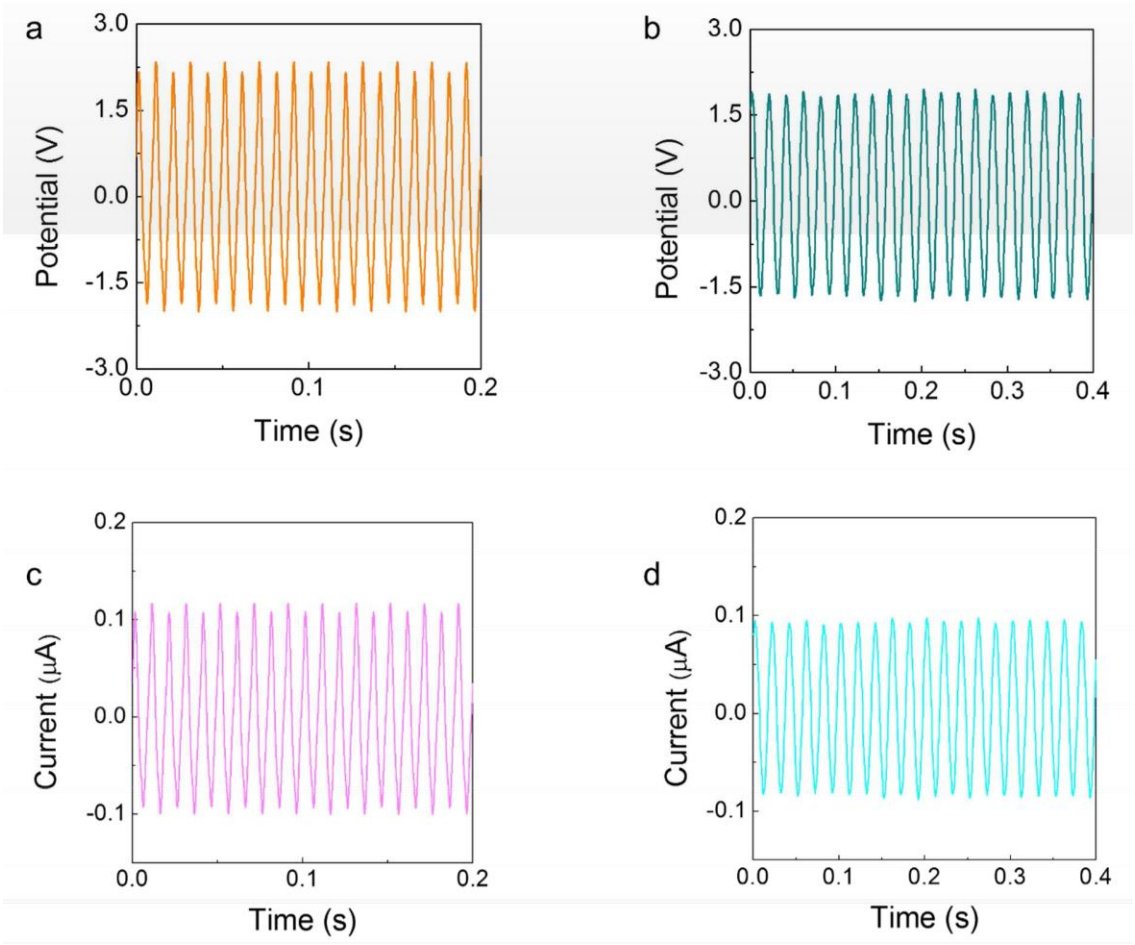


**Supplementary Figure S2.** Potential and current output of the TENG which was driven by environmental energy sources; (a) and (c) sound, and (b) and (b) wind, respectively.

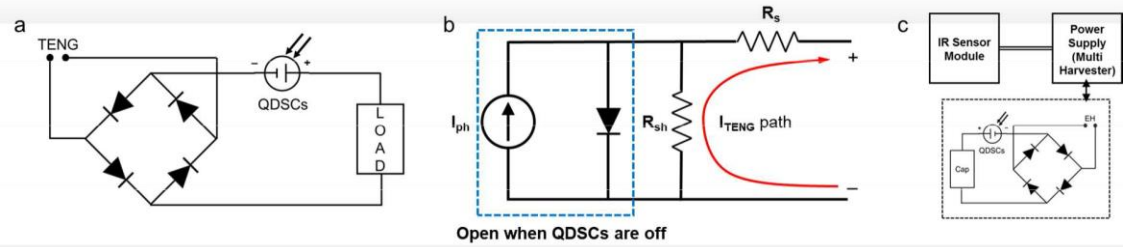


**Supplementary Figure S3.** (a) Schematics of a power management circuit for the HEH to obtain a hybrid signal. (b) An equivalent circuit of a solar cell and current path (Red curve) of the TENG ($I_{TENG}$). (c) The schematics of a sensor module connected with the power management circuit.

**Supplementary Video S1.** Operating LEDs at the conditions of charging capacitors and opening the relay switch for 0.2 seconds.

**Supplementary Video S2.** Operating LEDs at the continuous mode.

**Supplementary Video S3.** Operating the IR sensor without aid of any external power supply.